Pressure Based Calculation Procedure for Viscous Flows at All Speeds in Arbitrary Configurations

K. C. Karki*
General Motors Corporation, Indianapolis, Indiana
and
S. V. Patankar†
University of Minnesota, Minneapolis, Minnesota

A calculation procedure for viscous flows at all Mach numbers has been described. The scheme has been developed for a nonorthogonal coordinate system. In order to handle both incompressible and compressible flows, pressure has been selected as a primary dependent variable in preference to density. The pressure field is evaluated using the compressible form of the SIMPLER algorithm. The accuracy of the proposed scheme has been assessed by comparing the results with experimental data or other numerical results available in the literature.

Nomenclature

a	= combined convection-diffusion coefficient
b	= source term in the discretization equation
c_1, c_2, c_3	= geometric relations between coordinate systems
d_e, d_n	= coefficients in the pressure equation
J	= Jacobian of the inverse coordinate transformation
p', p''	= pressure corrections
p	= pressure
u, v	= Cartesian velocity components
u_ξ, u_η	= velocity components along ξ, η coordinate directions
U, V	= contravariant velocity components
V	= velocity vector
x, y	= Cartesian coordinates
$\alpha_\xi, \beta_\xi, \alpha_\eta, \beta_\eta$	= geometrical quantities, Eqs. (24–27)
ϕ	= dependent variable
ξ, η	= axes of curvilinear coordinates
ρ	= density
Γ	= diffusivity

Subscripts

e, w, n, s	= east, west, north, and south faces of a control volume
E, W, N, S	= east, west, north, and south neighbors of the grid point P
P	= pertaining to the grid point P
u, v	= pertaining to the velocity components u and v

Background

THE computation methods developed for solving the viscous fluid flow problems traditionally have been classified as methods for incompressible flows and those for compressible flows. The methods developed for incompressible flows are generally characterized by the use of pressure as a main dependent variable and a staggered grid arrangement to prevent a checkerboard pressure pattern.[1] The schemes for compressible flows, on the other hand, employ density as a primary variable and extract pressure from an equation of state.[2-4] Further, most of these methods are based on a nonstaggered grid in which all variables are stored at the same location. These schemes cannot be used for incompressible or low Mach number flows, because in these situations the density changes are very small and the pressure-density coupling becomes very weak. Efforts have been made to alleviate this difficulty by adding a fictitious density term as the time derivative term in the continuity equation.[5,6] A time marching scheme is then used to compute pressure via a fictitious equation of state. The solution is valid only when a steady state is reached. Such a scheme, however, cannot be employed to predict situations in which mixed compressible and incompressible flows are encountered.

A method that uses pressure as a primary dependent variable is free from the aforementioned difficulties encountered with the density-based methods. This is due to the fact that pressure changes are always finite, irrespective of the flow Mach number. Thus, the use of pressure as a primary variable allows the development of a calculation procedure that is valid for the entire spectrum of Mach numbers.

In this paper, details of a recently developed calculation procedure are presented.[7] The method is based on the steady-state form of the Navier-Stokes equations, unlike the unsteady form used in the density-based methods. Other efforts in this area include the work of Hah,[8] Rhie,[9] and Issa.[10] The present work, however, has many unique features. It is based on a staggered grid arrangement so that no difficulties are encountered in the evaluation of pressure. The method has been developed for generalized nonorthogonal coordinates and uses the velocity components along the grid lines as the dependent variables in the momentum equations. To avoid complicated tensor algebra, the discretization equations for these velocity components are obtained using an algebraic manipulation of the discretization equations for the Cartesian velocity components. Further, the effect of pressure on density has been implicitly included in the equations. The scheme is based on the compressible form of the SIMPLER algorithm.[1,11]

Governing Equations

The steady-state form of the differential equations governing the conservation of mass, momentum, energy, and other scalars, such as the kinetic energy of turbulence, can be cast into a general form as[12]

Presented as Paper 88-0058 at the AIAA 26th Aerospace Sciences Meeting, Reno, NV, Jan. 11-14, 1988; received Jan. 25, 1988; revision received Sept. 23 1988.

*Senior Research Scientist, Allison Gas Turbine Division.
†Professor, Department of Mechanical Engineering.

$$\frac{1}{J}\frac{\partial}{\partial\xi}(\rho U\phi)+\frac{1}{J}\frac{\partial}{\partial\eta}(\rho V\phi)$$
$$=\frac{1}{J}\frac{\partial}{\partial\xi}\left[\frac{\Gamma}{J}\left(c_1\frac{\partial\phi}{\partial\xi}-c_2\frac{\partial\phi}{\partial\eta}\right)\right]$$
$$+\frac{1}{J}\frac{\partial}{\partial\eta}\left[\frac{\Gamma}{J}\left(c_3\frac{\partial\phi}{\partial\eta}-c_2\frac{\partial\phi}{\partial\xi}\right)\right]+S \tag{1}$$

where

$$U=u\frac{\partial y}{\partial\eta}-v\frac{\partial x}{\partial\eta} \tag{2}$$

$$V=v\frac{\partial x}{\partial\xi}-u\frac{\partial y}{\partial\xi} \tag{3}$$

$$c_1=\left(\frac{\partial x}{\partial\eta}\right)^2+\left(\frac{\partial y}{\partial\eta}\right)^2 \tag{4}$$

$$C_2=\frac{\partial x}{\partial\xi}\frac{\partial x}{\partial\eta}+\frac{\partial y}{\partial\xi}\frac{\partial y}{\partial\eta} \tag{5}$$

$$c_3=\left(\frac{\partial x}{\partial\xi}\right)^2+\left(\frac{\partial y}{\partial\xi}\right)^2 \tag{6}$$

$$J=\frac{\partial x}{\partial\xi}\frac{\partial y}{\partial\eta}-\frac{\partial y}{\partial\xi}\frac{\partial x}{\partial\eta} \tag{7}$$

In this equation, ϕ is a general dependent variable and $S(\xi,\eta)$ is the source term of ϕ in the (ξ,η) coordinates.

Discretization of the Equations

General Scalar

The discretization equations are obtained by integrating the governing equations over a control volume. For a typical control volume around the point P, shown in Fig. 1, the integration of Eq. (1) with $\Delta\xi=\Delta\eta=1$ gives

$$\left[\rho U\phi-\Gamma\frac{c_1}{J}\frac{\partial\phi}{\partial\xi}\right)_e-\left[\rho U\phi-\Gamma\frac{c_1}{J}\frac{\partial\phi}{\partial\xi}\right]_w$$
$$+\left[\rho V\phi-\Gamma\frac{c_3}{J}\frac{\partial\phi}{\partial\eta}\right]_n-\left[\rho V\phi-\Gamma\frac{c_3}{J}\frac{\partial\phi}{\partial\eta}\right]_s$$
$$=\left(\Gamma\frac{c_2}{J}\frac{\partial\phi}{\partial\eta}\right)_w-\left(\Gamma\frac{c_2}{J}\frac{\partial\phi}{\partial\eta}\right)_e$$
$$+\left(\Gamma\frac{c_2}{J}\frac{\partial\phi}{\partial\xi}\right)_s-\left(\Gamma\frac{c_2}{J}\frac{\partial\phi}{\partial\xi}\right)_n+SJ \tag{8}$$

Equation (8) involves the values and the gradients of the dependent variable at the control-volume faces. This requires an assumption about the variation of ϕ between two grid points. For the terms on the left-hand side, which are treated implicitly, the power-law profile of Patankar[1,11] is used. A linear ϕ distribution is assumed for the terms on the right-hand side, which are treated in an explicit manner. It should be noted that the explicit terms are purely diffusive and should be small for high Reynolds number flows. The final discretized equation can be expressed as

$$a_P\phi_P=a_E\phi_E+a_W\phi_W+a_N\phi_N+a_S\phi_S+b \tag{9}$$

where the a_E, a_W, etc., denote the combined convection-diffusion coefficients and b includes all the terms calculated explicitly, including the source terms.

Momentum Equations

The above discretization procedure can be used for all variables if the expression for the source term $S(\xi,\eta)$ is available. The source terms for the scalars can be easily derived. But, due to the vector nature of the momentum equations, the complexity of the source terms for the velocity components varies with the choice of the reference coordinate system to which these components belong. For example, for the Cartesian velocity components the governing equations are very similar to those for a scalar. However, the governing equations for the curvilinear velocity components, such as the contravariant or the covariant components, involve additional curvature terms that arise due to the fact that these components do not have a fixed direction, and momentum is conserved along a straight line.

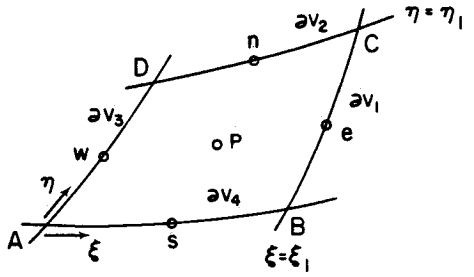

Fig. 1 Basic element for a finite-volume method.

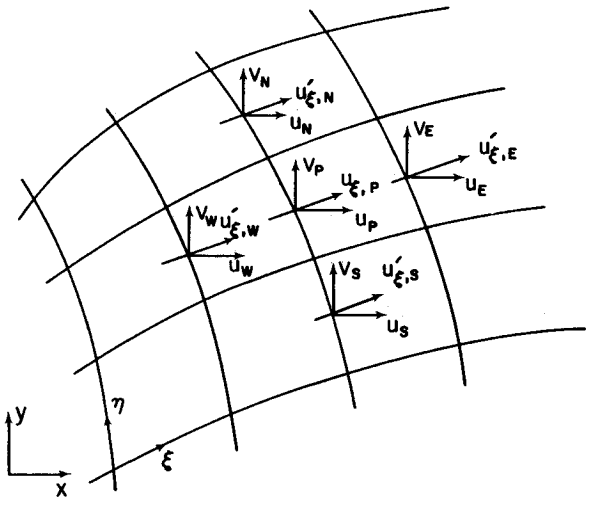

Fig. 2 Grid configuration with Cartesian velocity components as the dependent variables.

Due to the rather simple form of their conservation equation, the Cartesian velocity components are the preferable choice for the dependent variables in the momentum equations. This practice, in conjunction with a nonstaggered grid arrangement, is used in almost all the methods developed for compressible flows and in a few methods for incompressible flows.[13,14] The use of a nonstaggered grid for incompressible flows leads to checkerboard pressure and/or velocity fields, unless some specialized techniques for coupling the velocity and pressure fields are devised. The use of the Cartesian velocity components in a staggered grid arrangement requires storing both velocity components at each face[15] or corner[16] of a control volume. This results in extra computational effort even in the regions where the grid is orthogonal. It should be noted that if only one velocity component is stored at each control-volume face,[8] the applicability of the scheme will depend on the orientation of the grid relative to the Cartesian reference frame.

To avoid the above difficulties with the use of the Cartesian velocity components, the projections of the velocity vector along the grid lines are chosen as the dependent variables in the present work. Since these velocity components are oriented along the grid lines, only one velocity component is stored at each control-volume face. The curvilinear velocity

components have been used by only a few researchers[17,18] because the resulting equations are very complicated. In the present work, however, the discretization equations for these velocity components are obtained by an algebraic manipulation of the corresponding equations for the Cartesian velocity components. This procedure avoids any reference to the differential form of the conservation equations for the curvilinear velocity components. The details of the discretization procedure for the momentum equations are now described.

With reference to Fig. 2, suppose that the dependent variables are the Cartesian velocity components located at the control-volume faces. Since the diffusivities for both these velocity components are the same and their differential equations are being integrated over the same control volume, the resulting discretization equations will have identical influence coefficients, except for the source terms. These equations can be written as

$$a_P u_P = a_E u_E + a_W u_W + a_N u_N + a_S u_S + b_u \tag{10}$$

$$a_P v_P = a_E v_E + a_W v_W + a_N v_N + a_S v_S + b_v \tag{11}$$

The velocity component along the ξ direction $u_{\xi,P}$ is related to u_P and v_P as

$$u_\xi = \boldsymbol{V} \cdot \boldsymbol{e}_\xi = \frac{\left(u\dfrac{\partial x}{\partial \xi} + v\dfrac{\partial y}{\partial \xi}\right)}{(c_3)^{1/2}} \tag{12}$$

If the finite difference approximations for u_P and v_P are substituted in Eq. (12), we obtain, after slight rearrangement,

$$a_P u_{\xi,P} = a_E u'_{\xi,E} + a_W u'_{\xi,W} + a_N u'_{\xi,N} + a_S u'_{\xi,S} + b'_{u_\xi} \tag{13}$$

where

$$u'_{\xi,E} = a_{11} u_E + a_{12} v_E \tag{14}$$

$$u'_{\xi,W} = a_{11} u_W + a_{12} v_W \tag{15}$$

$$u'_{\xi,N} = a_{11} u_N + a_{12} v_N \tag{16}$$

$$u'_{\xi,S} = a_{11} u_S + a_{12} v_S \tag{17}$$

$$b'_{u_\xi} = a_{11} b_u + a_{12} b_v \tag{18}$$

with

$$a_{11} = \frac{(\partial x/\partial \xi)_P}{(c_3)_P^{1/2}}$$

$$a_{12} = \frac{(\partial y/\partial \xi)_P}{(c_3)_P^{1/2}}$$

From Eqs. (14–17), the primed velocities are recognized as the velocity components parallel to u_ξ at the neighboring points.

It is seen that the primed velocity components such as $u'_{\xi,E}$ are combinations of $u_{\xi,E}$ and $u_{\eta,E}$ and the above formulation, as such, would not permit a field solution for the velocities used as the dependent variables. This difficulty can be easily removed by introducing the "actual" neighbors (e.g., $u_{\xi,E}$) in the discretization equation, as follows:

$$\begin{aligned} a_P u_{\xi,P} = {} & a_E u_{\xi,E} + a_W u_{\xi,W} + a_N u_{\xi,N} + a_S u_{\xi,S} \\ & + b'_{u_\xi} \\ & + a_E(u'_{\xi,E} - u_{\xi,E}) \\ & + a_W(u'_{\xi,W} - u_{\xi,W}) \\ & + a_N(u'_{\xi,N} - u_{\xi,N}) \\ & + a_S(u'_{\xi,S} - u_{\xi,S}) \end{aligned} \tag{19}$$

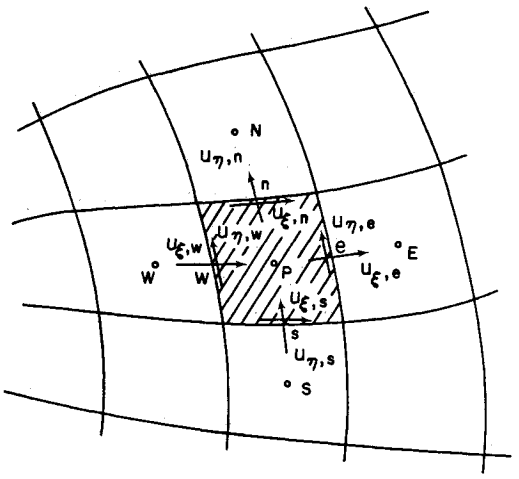

Fig. 3 Typical continuity control volume.

In Eq. (19), terms such as $a_E(u'_{\xi,E} - u_{\xi,E})$ and similar terms in the source term b'_{u_ξ} represent the effect of curvature and are equivalent to the discretized source terms, which would have resulted from tensor analysis. These terms are treated in an explicit manner.

For later reference, Eq. (19) is rewritten for the velocity component $u_{\xi,e}$ in Fig. 3, with the pressure gradient term appearing explicitly, as follows:

$$a_e u_{\xi,e} = \sum a_{nb} u_{\xi,nb} + A_e(p_P - p_E) + b_{u_\xi} \tag{20}$$

where the summation is over the four neighbors of e and b_{u_ξ} now includes all terms calculated explicitly.

Continuity Equation

The integrated continuity equation for a control volume around the grid point P, shown in Fig. 3, can be written as

$$(\rho U)_e - (\rho U)_w + (\rho V)_n - (\rho V)_s = 0 \tag{21}$$

where U and V are the contravariant velocity components defined earlier. These can be expressed in terms of the velocity components u_ξ and u_η, as follows:

$$U = \alpha_\xi u_\xi - \beta_\xi u_\eta \tag{22}$$

$$V = \alpha_\eta u_\eta - \beta_\eta u_\xi \tag{23}$$

where

$$\alpha_\xi = \frac{c_1}{J}(c_3)^{1/2} \tag{24}$$

$$\beta_\xi = \frac{c_2}{J}(c_1)^{1/2} \tag{25}$$

$$\alpha_\eta = \frac{c_3}{J}(c_1)^{1/2} \tag{26}$$

$$\beta_\eta = \frac{c_2}{J}(c_3)^{1/2} \tag{27}$$

Due to our decision to have pressure as a primary dependent variable, the continuity equation must be converted into an equation for pressure or a related quantity. This is done by combining the discretized continuity and momentum equations. In the present work, a compressible form of the SIMPLER algorithm has been used. In this procedure, two pressure correction equations are solved. The first pressure correction (p') is used to update the existing pressure and density fields; the second pressure correction (p'') is used to

correct the velocity field to ensure continuity of mass. The main steps in the derivation of equations for these pressure corrections are presented next. Full details are available in Ref. 7. The p'' equation is considered first.

p''-equation

The velcoity field obtained after solving the momentum equations, with the existing density and pressure fields, will not, in general, satisfy the continuity equation. This implies that the current pressure field is imperfect and a correction p'' must be added to it. The velocities and density react to this change in pressure as follows:

$$u''_{\xi,e} = d_e(p''_P - p''_E), \qquad d_e = \frac{A_e}{a_e} \tag{28}$$

$$\rho'' = K''p, \qquad K = \frac{\partial \rho}{\partial p} \tag{29}$$

The quantity K represents a measure of the influence of pressure on density and can be obtained from the equation of state. The value of K depends on the assumption used in the evaluation of the partial derivative in Eq. (29). For the results presented here, the fluid is assumed to undergo an isentropic process, so that K is the inverse of the square of the speed of sound. Other alternatives, such as an isothermal process, also can be used. However, it should be noted that upon convergence the pressure (hence density) changes will vanish, and the final result will be independent of the precise choice for K.

The mass flux through a control-volume face (for example, e) is given by

$$(\rho U)_e = (\alpha_\xi \rho u_\xi)_e - (\beta_\xi \rho^* u^o_\eta)_e \tag{30}$$

where superscript 'o' denotes values from the previous iteration and the starred quantities are the currently available values.

The product (ρu_ξ) in the first term in Eq. (30) can be expressed as

$$\begin{aligned} \rho u_\xi &= (\rho^* + \rho'')(u^*_\xi + u''_\xi) \\ &= \rho^* u^*_\xi + \rho^* u''_\xi + \rho'' u^*_\xi \end{aligned} \tag{31}$$

In Eq. (31), the second order term $\rho'' u''_\xi$ has been omitted. Replacing the velocity and density changes in terms of pressure changes, the mass flux can be expressed as

$$\begin{aligned} (\rho U)_e &= (\alpha_\xi \rho^* u^*_\xi)_e + \alpha_{\xi,e} \rho^*_e d_e (p''_P - p''_E) \\ &\quad + \alpha_{\xi,e} u^*_{\xi,e} \rho''_e - (\beta_\xi u^o_\eta \rho^*)_e \end{aligned} \tag{32}$$

At this stage, a decision must be made about the value of density at a control-volume face. In this regard, it should be noted that in compressible flows the continuity equation acts as a transport equation for density. Thus, the interpolation for density should be similar to that for a scalar, but with Mach number as the governing parameter instead of the Peclet number. An additional requirement on the density interpolation is that, in conjunction with the differencing of the pressure gradient term, it should yield a pressure or pressure correction equation that exhibits the correct Mach number dependent behavior. That is, the character of the resulting equation should be elliptic in the subsonic flow regime and hyperbolic in the supersonic regime. Further, the transition from subsonic to supersonic flow should be smooth.

In the present study, a first-order upwinding has been employed for density and the pressure gradient term is always discretized using central differencing. Use of upstream density also has been suggested by Patankar[19] and Issa and Lockwood.[20] With this, the expressions for density and density corrections at the interfaces are

$$\rho_e = \rho_p \frac{\max[u_{\xi,e,0}]}{u_{\xi,e}} + \rho_E \frac{\max[-u_{\xi,e,0}]}{u_{\xi,e}} \tag{33}$$

$$\rho''_e = \rho''_P \frac{\max[u_{\xi,e,0}]}{u_{\xi,e}} + \rho''_E \frac{\max[-u_{\xi,e,0}]}{u_{\xi,e}} \tag{34}$$

It should be mentioned that the nature of the pressure correction equation in the present formulation is very similar to that of the compressible potential equation, and the practice of density upwinding along with central differencing for the potential gradient term is very widely used in potential flow calculations (e.g., Refs. 21–23). Such a differencing scheme results in the correct Mach number dependent behavior for pressure.

The dependence of pressure on mass flux can be illustrated by using a one-dimensional situation for which Eqs. (32–34) can be combined to give

$$(\rho u)_e = (\rho u)^*_e + \rho^*_p d_e (p''_P - p''_E) + u^*_e K_P p''_p \tag{35}$$

In Eq. (35), the diffusion-like term involving d_e is responsible for the downstream pressure effects, whereas the convective term involving K_p brings the upstream effects. It can be readily shown that the ratio $(\rho^*_P d_e / u^*_e K_P)$ is inversely proportional to the square of the Mach number. At low Mach numbers, the term involving the pressure difference is dominant, and the equation exhibits the elliptic nature of pressure. As the Mach number increases, the influence of upstream pressure becomes more dominant, and the hyperbolic nature of flow is recovered.

The continuity equation now can be written as

$$a_P p''_P = a_E p''_E + a_W p''_W + a_N p''_N + a_S p''_S + b + b_{NO} \tag{36}$$

where

$$a_E = \alpha_{\xi,e}(\rho^*_e d_e + K_E \max[-u^*_{\xi,e}, 0]) \tag{37}$$

$$a_W = \alpha_{\xi,w}(\rho^*_w d_w + K_W \max[u^*_{\xi,w}, 0]) \tag{38}$$

$$a_N = \alpha_{\eta,n}(\rho^*_n d_n + K_N \max[-u^*_{\eta,n}, 0]) \tag{39}$$

$$a_S = \alpha_{\eta,s}(\rho^*_s d_s + K_S \max[u^*_{\eta,s}, 0]) \tag{40}$$

$$\begin{aligned} a_p = {} & \alpha_{\xi,e}(\rho^*_e d_e + K_P \max[u^*_{\xi,e}, 0]) \\ & + \alpha_{\xi,w}(\rho^*_w d_w + K_P \max[-u^*_{\xi,w}, 0]) \\ & + \alpha_{\eta,n}(\rho^*_n d_n + K_P \max[u^*_{\eta,n}, 0]) \\ & + \alpha_{\eta,s}(\rho^*_s d_s + K_P \max[-u^*_{\eta,s}, 0]) \end{aligned} \tag{41}$$

$$\begin{aligned} b = {} & -[(\alpha_\xi \rho^* u^*_\xi)_e - (\alpha_\xi \rho^* u^*_\xi)_w \\ & + (\alpha_\eta \rho^* u^*_\eta)_n - (\alpha_\eta \rho^* u^*_\eta)_s] \end{aligned} \tag{42}$$

$$\begin{aligned} b_{NO} = {} & (\beta_\xi \rho^* u^o_\eta)_e - (\beta_\xi \rho^* u^o_\eta)_w \\ & + (\beta_\eta \rho^* u^o_\xi)_n - (\beta_\eta \rho^* u^o_\xi)_s \end{aligned} \tag{43}$$

It should be noted that with $K = 0$, the above equations are valid for incompressible flows also. The formulation of the pressure correction equation is now complete, and a few comments about its solution need to be made. First, the nonorthogonal terms, which involve the velocities along the control-volume faces, should be calculated using the continuity-satisfying velocity field from the previous iteration. Such a practice exhibits a much better convergence behavior compared to a method in which the currently available imperfect velocities (from the solution of the momentum equations) are used to calculate these terms. By lagging these terms by one iteration, the continuity equation cannot be satisfied implicitly, if solved only once. To avoid this difficulty, the pressure correction equation is solved two or three times.

Second, in the derivation of the pressure correction equation, the second order term $\rho'' u''_{\xi}$ was ignored. Consequently, if the updated velocities and densities are used to calculate mass flow rates, these will not satisfy the continuity equation exactly. In order to obtain flow rates that would ensure the conservation of mass, it is preferable to correct the flow rates themselves rather than to obtain them from the corrected velocity and density fields.

p'-equation

The steps in the derivation of the first pressure correction (p') equation are similar to those for the p'' equation outlined above. The purpose of p' equation is to correct the existing pressure and density fields. In the derivation of p'' equation, the discretized continuity equation was combined with a truncated form of the momentum equations. Now, the full momentum equations, e.g., Eq. (20), are used and the starred velocities used earlier are replaced by the pseudovelocities, defined as follows:

$$\hat{u}_{\xi,e} = \frac{\Sigma a_{nb} u_{\xi,nb} + b_{u_\xi}}{a_e} + d_e(p_P^* - p_E^*) \tag{44}$$

$$\hat{u}_{\eta,n} = \frac{\Sigma a_{nb} u_{\eta,nb} + b_{u_\eta}}{a_n} + d_n(p_P^* - p_N^*) \tag{45}$$

Therefore, the source term b in p' equation is calculated using the pseudovelocities rather than the actual velocities. In addition, since the convective terms now involve the pseudovelocities, the upwinding of density is also decided by these velocities. However, the source term b_{NO} arising due to nonorthogonality of the coordinate system should still be based on the actual velocities.

Overall Solution Procedure

At this point all the ingredients of the calculation procedure are available and may be assembled. The sequence of steps is as follows:

1) The density values are obtained from the current pressure and temperature fields.

2) The coefficients and source terms for the momentum equations are calculated from the available values of various variables.

3) The first pressure correction (p') equation is solved. This is used to correct the existing pressure and density fields.

4) With the updated pressures, the momentum equations are solved. These velocities, in general, will not satisfy the continuity equation.

5) The second pressure correction (p'') equation is solved, and the flow rates and velocities are corrected.

6) The enthalpy equation is solved and temperature field is extracted from the solution.

7) Steps 1 through 6 are repeated until convergence is reached.

Applications

The present calculation procedure has been used to solve a variety of problems.[7] These include inviscid compressible flows and viscous (laminar and turbulent) incompressible and compressible flows. Here the emphasis is on compressible flows, and only one example of incompressible flow will be presented. The performance of the present scheme is evaluated by comparing the results with experimental data or with other numerical results available in literature.

Flow in a Channel with a Bump

The capability of the present method is demonstrated by computing inviscid flow in a channel with a bump on the lower wall. This test case has been used by various researchers to test their schemes.[24,25]

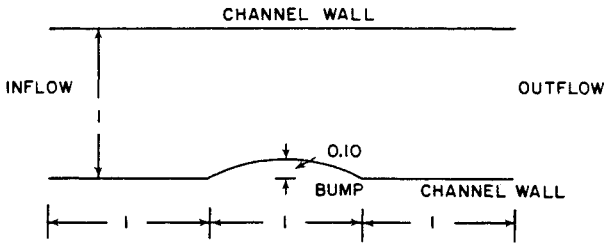

Fig. 4 Channel with a circular arc "bump."

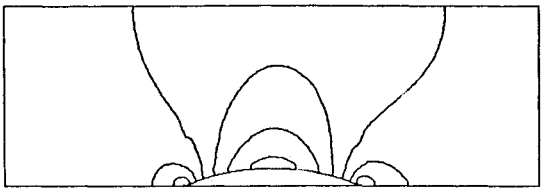

Fig. 5 Isomach lines for subsonic flow.

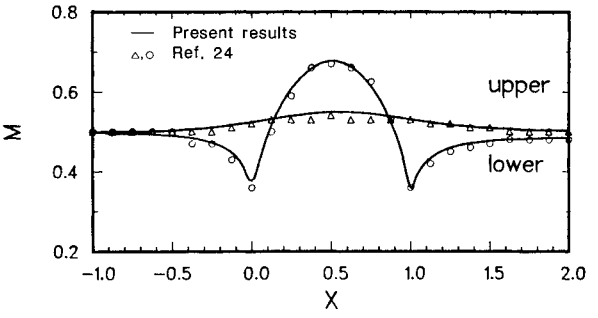

Fig. 6 Surface Mach number distribution for subsonic flow: comparison with second-order Gudonov scheme.[24]

(1) *Subsonic Flow*

The channel under consideration is shown in Fig. 4. It has a 10% thick circular arc "bump" on the lower wall. The distance between the walls is equal to the chord length of the bump. Results have been obtained using a 62×22 nonuniform sheared grid. The grid lines are closely packed in and near the bump region.

Boundary Conditions

At the inlet, total temperature, total pressure, and the transverse velocity component are specified. At the exit, the static pressure is specified. This imposed isentropic static-to-stagnation pressure ratio implies a Mach number of 0.5. Along the solid surfaces of the computational domain, the tangency condition is applied. The stagnation enthalpy is assumed to be constant in the computational domain.

Results

Figures 5 and 6 show the isomach lines and the Mach number distribution along the walls, respectively. The computed solution is very symmetric about the midchord, which is a good indication of the accuracy of the scheme for this subsonic flow application.

Figure 6 also shows the numerical results of Eidelman et al.[24] using the second-order Gudonov scheme. The agreement between the two sets of results is very good. It should be mentioned that the level of agreement between the present results and others available in literature (e.g., Ref. 25) is very similar to that shown in Fig. 6.

(2) *Transonic Flow*

In this section, results for transonic flow in the same channel with 10% thick arc bump are presented. The imposed static-to-stagnation pressure ratio implies a Mach number of 0.675 in this case. The grid arrangement and the treatment of boundary conditions are identical to those described for the subsonic flow presented above.

Results

The isomach lines and the Mach number distributions for this flow situation are shown in Figs. 7 and 8, respectively. Now, a supersonic region appears in the solution which is terminated by a shock. The numerical results of Eidelman et al.[24] using the first-order Gudonov scheme are also shown in Fig. 8. It is seen that the present method underpredicts the shock strength by about 10%; the maximum Mach number predicted by the present method is 1.1, as opposed to about 1.2 obtained using the Gudonov scheme. The use of a second-order scheme such as MacCormack's[25] or Gudonov's[24] results in a still higher shock strength. As expected, in the regions away from the shock, results obtained using different schemes are in good agreement with each other.

The underprediction of the shock strength indicates excessive dissipation in the vicinity of the shock wave. In the present computational scheme, there are two sources of numerical diffusion: the upwinding of convective terms in the momentum equations, and the upwinding of density in the continuity equation. These two effects are probably producing more dissipation than is necessary to stabilize the solution. This shortcoming can be remedied by using higher order upwind schemes. Efforts in this direction are currently under way.

(3) *Supersonic Flow*

For supersonic flow, a channel with a 4% thick arc bump with an inlet Mach number of 1.65 was considered. This particular configuration was considered to facilitate the comparison of the present results with those obtained by Eidelman et al.[24] using the first-order Gudonov scheme.

The computations were performed on a 67×22 sheared grid similar to that used in the previous two calculations. At the inflow boundary all variables were specified, whereas all variables were extrapolated at the exit.

Results

The isomach lines and the Mach number distribution on the walls for this case are shown in Figs. 9 and 10. To facilitate comparison, the Mach number distribution obtained by Eidelman et al.[24] using a first-order scheme are also presented. It is observed that there is an oblique shock wave leaving the leading edge. This leading-edge shock intersects the top wall and is reflected back to intersect with the shock leaving the trailing edge. The results from the present scheme exhibit this behavior, but the resolution of the complex shock structure is not very good due to smearing of the shock waves. Use of a higher order scheme would produce a better description of this flow situation.

Planar Supersonic Nozzle

In this section, results are presented for a planar nozzle (B-1) reported by Mason et al.[26] The geometrical details for this test case are given in Fig. 11. Computations have been performed using both the (laminar) Navier-Stokes equations and the Euler equations. The pressure distribution at the wall and the centerline are compared with the experimental data,[26] which were taken at the midspan of the duct walls and on the centerline of the endwalls.

Computational Details

The numerical results have been obtained using a 47×12 sheared grid for the half-nozzle. The grid spacing was uniform in the transverse direction. In the axial direction, however, more grid points were placed near the throat.

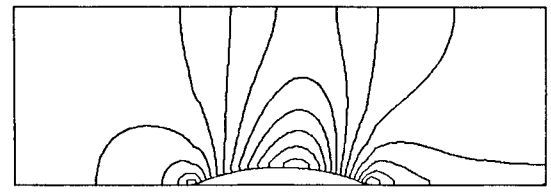

Fig. 7 Isomach lines for transonic flow.

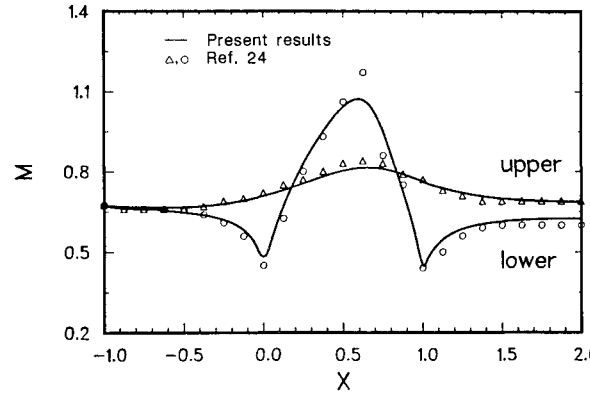

Fig. 8 Surface Mach number distribution for transonic flow: comparison with first-order Gudonov scheme.[24]

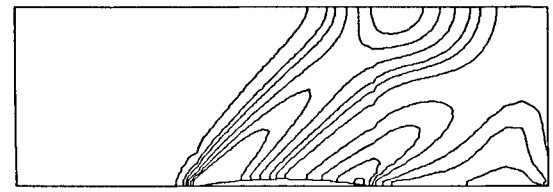

Fig. 9 Isomach lines for supersonic flow.

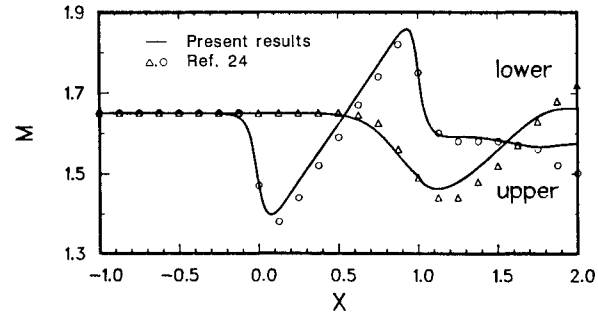

Fig. 10 Surface Mach number distribution for supersonic flow: comparison with first-order Gudonov scheme.[24]

The treatment of boundary conditions for the Euler equations was presented above. For the Navier-Stokes equations, the no-slip condition was used at the walls, instead of the tangency condition. The inlet Mach number was taken as 0.232 and the ratio of the exit static pressure to the upstream stagnation pressure was fixed at 0.1135, corresponding to the design condition.

Results

Figures 12–14 show the solution to the Euler equations. The agreement between the numerical results and the experimental data is seen to be very good at both the nozzle wall and the centerline positions.

The viscous calculations were performed at a Reynolds number of 7.5×10^6, based on the inlet half nozzle width and

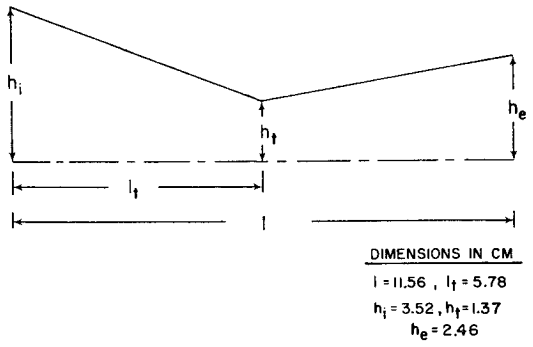

Fig. 11 Planar converging-diverging nozzle.

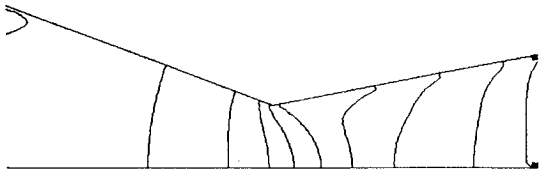

Fig. 12 Isomach lines for the inviscid case, $M = 0.2(0.2)2.0$.

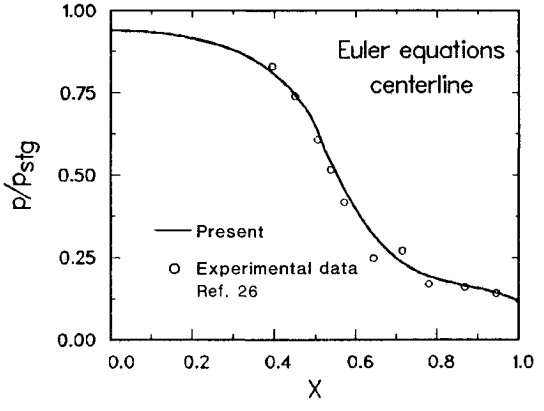

Fig. 13 Pressure distribution at the centerline using the Euler equations.

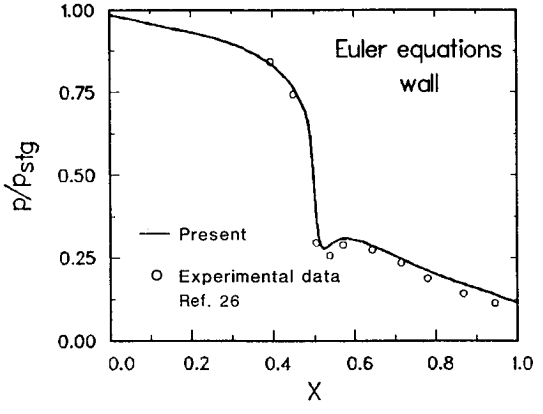

Fig. 14 Pressure distribution at the wall using the Euler equations.

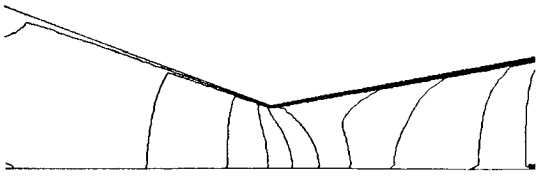

Fig. 15 Isomach lines for the viscous case, $M = 0.2(0.2)2.0$.

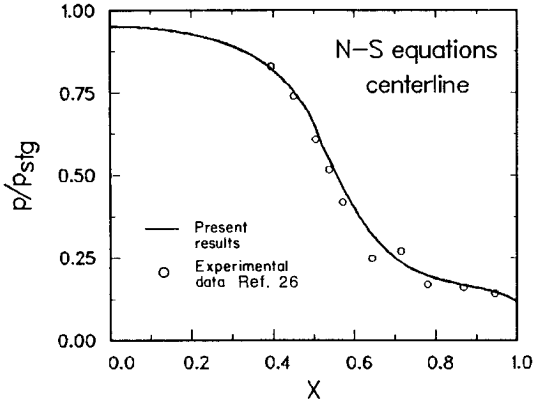

Fig. 16 Pressure distribution at the centerline using the Navier-Stokes equations.

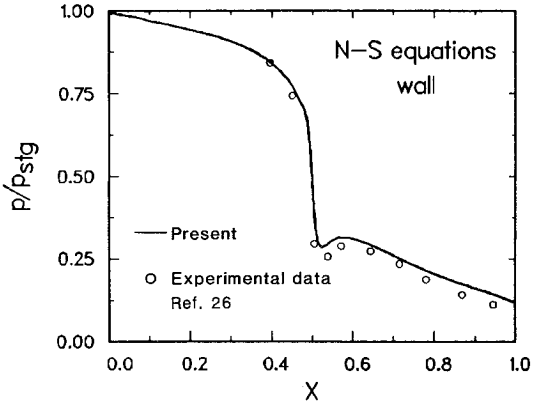

Fig. 17 Pressure distribution at the wall using the Navier-Stokes equations.

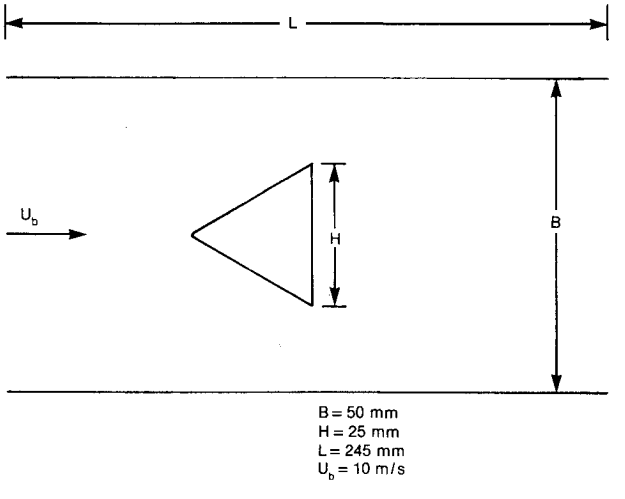

Fig. 18 Wedge-shaped flameholder setup.

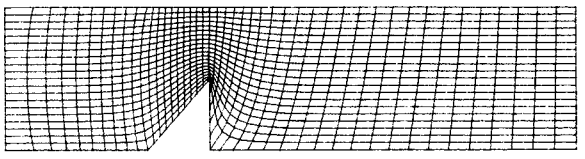

Fig. 19 Grid for the flameholder setup (not to scale).

the critical speed. The results are shown in Figs. 15–17. Again, the level of agreement between the computed results and the experimental data is very good.

Flow Around a Wedge-Shaped Flameholder

The capability of the proposed scheme to compute incompressible flows is demonstrated by computing the turbulent flow behind a wedge-shaped flame stabilizer shown in Fig. 18. This flow situation was studied experimentally by Fuji et al.[27] with the aid of laser Doppler velocimetry. The flame stabilizer was an equilateral triangle in cross section with each side (H) being 25 mm for an average freestream velocity of 10 m/s. The measured parameters were

$$\text{Length of the recirculation zone} = 2.2\,H$$
$$\text{Amount of air being recirculated} = 0.1\,m_{\text{in}}$$
$$\text{Maximum reverse flow velocity} = 0.4\,U_b$$

where

m_{in} = inlet air flow rate
U_b = freestream velocity

This case was computed using the present scheme in conjunction with the two-equation model of turbulence.[28] Results were obtained using a 47×22 grid shown in Fig. 19. The grid was generated by solving a set of elliptic equations.[29] Due to the symmetry of the problem, computations were performed only for one-half of the setup. The predicted parameters are

$$\text{Length of the recirculating zone} = 2.1\,H$$
$$\text{Amount of air being recirculated} = 0.11\,m_{\text{in}}$$
$$\text{Maximum reverse flow velocity} = 0.5\,U_b$$

which are in good agreement with the measurements.

Concluding Remarks

In this paper, a general method for computing compressible and incompressible flows has been presented. The calculation procedure is based on a control-volume approach with a staggered grid arrangement. The momentum equations are cast in terms of the physical velocity components along the grid lines, and pressure is retained as a main dependent variable in preference to density. The method has been used to solve a variety of incompressible and compressible flows, ranging from subsonic to supersonic. The results are in good agreement with those available in the literature except in the vicinity of a shock, which is smeared due to excessive numerical dissipation. Efforts are being undertaken to improve the shock capturing capability of the method.

References

[1]Patankar, S. V., *Numerical Heat Transfer and Fluid Flow*, Hemisphere, Washington, DC 1980.

[2]Beam, R. M. and Warming, R. F., "An Implicit Factored Scheme for Compressible Navier-Stokes Equations," *AIAA Journal*, Vol. 16, April 1978, pp. 87–110.

[3]Briley, W. R. and McDonald, H., "Solution of the Multidimensional Navier-Stokes Equations by a Generalized Implicit Method," *Journal of Computational Physics*, Vol. 24, 1977, pp. 373–397.

[4]MacCormack, R. W., "A Numerical Method for Solving the Equations of Compressible Viscous Flows," *AIAA Journal*, Vol. 20, Sept. 1982, pp. 1275–1281.

[5]Kwak, D., Chang, J. L. C., Shanks, S. P., and Chakravarthy, S. R., "A Three-Dimensional Incompressible Navier-Stokes Flow Solver Using Primitive Variables," *AIAA Journal*, Vol. 24, March 1986, pp. 390–396.

[6]Chang, J. L. C. and Kwak, D., "On the Method of Pseudo-Compressibility for Numerically Solving Incompressible Flows," AIAA Paper 84-0252, Jan. 1984.

[7]Karki, K. C., "A Calculation Procedure for Viscous Flows at All Speeds in Complex Geometries," Ph.D. Thesis, Univ. of Minnesota, Minneapolis, MN, 1986.

[8]Hah, C., "A Navier-Stokes Analysis of Three-Dimensional Turbulent Flows Inside Turbine Blade Rows at Design and Offdesign Conditions," *Journal of Engineering for Gas Turbines and Power*, Vol. 106, 1984, pp. 383–390.

[9]Rhie, C. M., "A Pressure Based Navier-Stokes Solver Using the Multigrid Method," AIAA Paper 86-0207, Jan. 1986.

[10]Issa, R. I., "Solution of the Implicitly Discretized Fluid Flow Equations by Operator-Splitting," *Journal of Computational Physics*, Vol. 62, 1986, pp. 40–65.

[11]Patankar, S. V., "A Calculation Procedure for Two-Dimensional Elliptic Situations," *Numerical Heat Transfer*, Vol. 4, 1981, pp. 409–425.

[12]Vinokur, M., "Conservation Equations of Gas Dynamics in Curvilinear Coordinate Systems," *Journal of Computational Physics*, Vol. 14, 1974, pp. 105–125.

[13]Rhie, C. M. and Chow, W. L., "Numerical Study of the Turbulent Flow Past an Airfoil with Trailing Edge Separation," *AIAA Journal*, Vol. 21, Nov. 1983, pp. 1525–1532.

[14]Reggio, M. and Camarero, R., "Numerical Solution Procedure for Viscous Incompressible Flows," *Numerical Heat Transfer*, Vol. 10, 1986, pp. 131–146.

[15]Maliska C. R. and Raithby, G. D., "A Method for Computing Three-Dimensional Flows Using Nonorthogonal Boundary-Fitted Coordinates," *International Journal for Numerical Methods in Fluids*, Vol. 4, 1984, pp. 518–537.

[16]Vanka, S. P., Chen, B. C.-J., and Sha, W. T., "A Semi-Implicit Calculation Procedure for Flow Described in Body-Fitted Coordinates," *Numerical Heat Transfer*, Vol. 3, 1980, pp. 1–19.

[17]Gal-Chen, T. and Sommerville, R. C. J., "Numerical Solution of the Navier-Stokes Equations with Topography," *Journal of Computational Physics*, Vol. 17, 1975, pp. 276, 310.

[18]Demirdzic I., Gosman, A. D., and Issa, R. I., "A Finite-Volume Method for the Prediction of Turbulent Flow in Arbitrary Geometries," *Lecture Notes in Physics*, Vol. 141, Springer-Verlag, Berlin, 1980, pp. 141–150.

[19]Patankar, S. V., "Calculation of Unsteady Compressible Flows Involving Shocks," Mechanical Engineering Dept., Imperial College, London, Rept. UF/TN/A/4, 1971.

[20]Issa, R. I. and Lockwood, F. C., "On the Prediction of Two-Dimensional Supersonic Viscous Interactions Near Walls," *AIAA Journal*, Vol. 15, Feb. 1977, pp. 182–188.

[21]Hafez, M., South, J. C., and Murman, E. M., "Artificial Compressibility Method for Numerical Solution of Transonic Full Potential Equation," *AIAA Journal*, Vol. 17, Aug. 1979, pp. 838–844.

[22]Holst, T. L. and Ballhaus, W. F., "Fast Conservative Schemes for Full Potential Equations Applied to Transonic Flows," *AIAA Journal*, Vol. 17, Feb. 1979, pp. 145–152.

[23]Wornom, S. F., "A Two-Point Difference Scheme for Computing Steady-State Solutions to the Conservative One-Dimensional Euler Equations," *Computers and Fluids*, Vol. 12, 1984, pp. 11–30.

[24]Eidelman, S., Collela, P., and Shreeve, R. P., "Application of the Gudonov Method and Its Extension to Cascade Flow Modeling," *AIAA Journal*, Vol. 22, Nov. 1984, pp. 1609–1615.

[25]Ni, R. H., "A Multiple-Grid Scheme for Solving the Euler Equations," *AIAA Journal*, Vol. 20, Nov. 1982, pp. 1565–1571.

[26]Mason, M. L., Putnam, L. E., and Re, R. J., "The Effect of Throat Contouring on Two-Dimensional Converging-Diverging Nozzles at Static Conditions," NASA TP 1704, 1980.

[27]Fuji, S., Gomi, M., and Eguchi, K., "Cold Flow Tests of a Bluff-Body Flame Stabilizer," *Journal of Fluids Engineering*, Vol. 100, 1978, pp. 323–332.

[28]Launder, B. E. and Spalding, D. B., "The Numerical Computation of Turbulent Flows," *Computer Methods in Applied Mechanics and Engineering*, Vol. 3, 1974, pp. 269–289.

[29]Thompson, J. F., Warsi, Z. U. A., and Mastin, C. W., *Numerical Grid Generation-Foundations and Applications*, Elsevier, New York, 1985.